arXiv:1510.00968v1 [astro-ph.SR] 4 Oct 2015

Chemical Imaging of the CO Snow Line in the HD 163296 Disk

Chunhua Qi[1], Karin I. Öberg[1], Sean M. Andrews[1], David J. Wilner[1], Edwin A. Bergin[2], A. Meredith Hughes[3], Michiel Hogherheijde[4], Paola D'Alessio[5,6]

ABSTRACT

The condensation fronts (snow lines) of H_2O, CO and other abundant volatiles in the midplane of a protoplanetary disk affect several aspects of planet formation. Locating the CO snow line, where the CO gas column density is expected to drop substantially, based solely on CO emission profiles is challenging. This has prompted an exploration of chemical signatures of CO freeze-out. We present ALMA Cycle 1 observations of the N_2H^+ $J = 3 - 2$ and DCO^+ $J = 4 - 3$ emission lines toward the disk around the Herbig Ae star HD 163296 at $\sim 0.5''$ (60 AU) resolution, and evaluate their utility as tracers of the CO snow line location. The N_2H^+ emission is distributed in a ring with an inner radius at 90 AU, corresponding to a midplane temperature of 25 K. This result is consistent with a new analysis of optically thin $C^{18}O$ data, which implies a sharp drop in CO abundance at 90 AU. Thus N_2H^+ appears to be a robust tracer of the midplane CO snow line. The DCO^+ emission also has a ring morphology, but neither the inner nor the outer radius coincides with the CO snow line location of 90 AU, indicative of a complex relationship between DCO^+ emission and CO freeze-out in the disk midplane. Compared to TW Hya, CO freezes out at a higher temperature in the disk around HD 163296 (25 vs. 17 K in the TW Hya disk), perhaps due to different ice compositions. This highlights the importance of actually measuring the CO snow line location, rather than assuming a constant CO freeze-out temperature for all disks.

Subject headings: protoplanetary disks; astrochemistry; stars: formation; ISM: molecules; techniques: high angular resolution; radio lines: ISM

[1]Harvard-Smithsonian Center for Astrophysics, 60 Garden Street, Cambridge, MA 02138, USA

[2]Department of Astronomy, University of Michigan, 500 Church Street, Ann Arbor, MI 48109, USA

[3]Van Vleck Observatory, Astronomy Department, Wesleyan University, 96 Foss Hill Drive, Middletown, CT 06459, USA

[4]Leiden Observatory, Leiden University, PO Box 9513, 2300 RA Leiden, The Netherlands

[5]Centro de Radioastronomía y Astrofísica, Universidad Nacional Autónoma de México, 58089 Morelia, Michoacán, México

[6]Deceased Nov 14, 2013

1. Introduction

A condensation front is the two-dimensional surface in a protoplanetary disk where abundant volatiles freeze out of the gas phase onto solid particles: the "snow line" marks this condensation front at the disk midplane. Based on observations of protostars and comets, as well as theoretical models of disk chemistry, the most important snow lines are due to H_2O, CO_2, CO and N_2 freeze-out (Öberg et al. 2011a; Mumma & Charnley 2011). At each of these snow lines there will be a substantial increase in particle size and solid surface density, augmented by cold finger and pressure trap effects, which may speed up planetesimal formation (Ciesla & Cuzzi 2006; Johansen et al. 2007; Chiang & Youdin 2010; Gundlach et al. 2011; Ros & Johansen 2013). Freeze-out of different volatiles will also affect grain stickiness, another key factor for particle growth in disks. The importance of an individual snow line on the planet formation process in a disk will depend on its radius with respect to the distribution of mass in the disk, i.e. the density profile. To evaluate the importance of different snow lines to planet formation therefore requires precise constraints on snow line locations. Snow line locations are also important for setting the bulk composition of planets. That is, where a planet accretes its core and envelope with respect to different snow lines will affect its solid and atmospheric C/O ratio, and therefore the planetary chemistry (Öberg et al. 2011b).

The locations of snow lines depend on the volatile composition (e.g. whether most nitrogen is in N_2 or NH_3), the balance between freeze-out and thermal and non-thermal desorption rates (which are themselves set by a combination of density, temperature, and radiation fields), and dynamical processes in the disk, including drift of grains and gas diffusion (Öberg et al. 2011c; Oka et al. 2012; Ali-Dib et al. 2014; Baillié et al. 2015). Exact snow line locations are therefore difficult to predict theoretically; observational constraints are key. Of the major snow lines, the CO one should be the most straightforward to constrain observationally using millimeter interferometry. CO is the most abundant molecule after H_2 and its snow line is theoretically expected in the outer disk, where the temperature reaches ∼20 K. In the disks around T Tauri and Herbig Ae stars, this threshold is at a radius of ∼20–150 AU, and can thus in principle be resolved with modern millimeter interferometers. In practice, the presence of warmer CO in the gas phase at larger heights above the midplane (in the disk atmosphere) at all radii makes it difficult to directly locate the CO snow line.

The most detailed attempt to date to use observations of CO emission lines to infer the CO snow line location was carried out by Qi et al. (2011) for the disk around HD 163296 at a distance of ∼122 pc, the target of this study. Qi et al. (2011) used the spectral energy distribution (SED) along with multiple optically thick ^{12}CO transitions to constrain the two-dimensional (radial and vertical) density and temperature structure of the disk. The CO snow line location was then constrained using the less optically thick ^{13}CO J=2 − 1 line emission, and found to be at a radius of 155 AU.

Another approach to constrain the CO snow line location is to exploit chemical effects that are

regulated by CO freeze-out (Qi et al. 2013a). One such method of tracing the CO snow line uses the ion N_2H^+ (Qi et al. 2013b). CO in the gas phase will significantly slow down N_2H^+ formation *and* speed up N_2H^+ destruction (Bergin et al. 2001). The predicted anti-correlation of gas-phase CO and N_2H^+ has been confirmed by observations in pre-stellar and protostellar environments (Caselli et al. 1999; Bergin et al. 2002; Jørgensen 2004). In disks, such anti-correlation should result in a N_2H^+ ring, where the inner ring radius traces the onset of CO freeze-out (i.e. CO depletion from the gas-phase) at the CO snow line. Qi et al. (2013b) imaged N_2H^+ emission from the disk around the T Tauri star TW Hya and found a large ring with an inner edge at 30 AU. Associating that inner ring location with the CO snow line, a CO freeze-out temperature of 17 K was extracted based on a detailed model for the disk density and temperature structure.

Mathews et al. (2013) advocate another tracer based on the distribution of the ion DCO^+. In most chemical models, the dominant DCO^+ formation pathway involves H_2D^+, which promotes an increasing DCO^+ abundance at low (<30 K) temperatures as long as CO is available in the gas phase. Therefore, the DCO^+ emission in a disk is expected to peak just *interior* to the CO snow line. Mathews et al. (2013) imaged DCO^+ emission toward the HD 163296 disk and found a ring morphology with an outer edge that coincides with the Qi et al. (2011) CO snow line of 155 AU, supporting this theory. However, more recent models suggest that other, warmer formation pathways of DCO^+ may be also important in disks, increasing the DCO^+ abundance in higher (warmer) disk layers and thus weakening the relationship between the DCO^+ abundance distribution and the midplane CO snow line (Favre et al. 2015).

In this article, we revisit the CO snow line in the disk around HD 163296. The aim is to determine the CO snow line location using observations of N_2H^+ emission. We also present archival $C^{18}O$ and new DCO^+ observations and compare the constraints provided by these different chemical tracers of the gas-phase distribution of CO. These data and their calibration are described in §2. We present the N_2H^+, DCO^+, and $C^{18}O$ emissions maps from the HD 163296 disk, along with their associated abundance profiles derived from models, in §3. The results are used to determine the CO snow line locations in this disk, and to evaluate the utility and robustness of these different probes, in §4.

2. Observations

The observations of N_2H^+ and DCO^+ from the HD 163296 disk were carried out with the Atacama Large Millimeter/submillimeter Array (ALMA) on 21 May 2014, with 32 12 m antennas (ALMA Cycle 1 project 2012.1.00681.S). The total integration time on HD 163296 was 45 minutes. Baselines ranged from 18–650 m (17–605 kλ).

The correlator was configured to observe four spectral windows (SPWs): two were centered at the rest frequencies of the N_2H^+ $J = 3 - 2$ and DCO^+ $J = 4 - 3$ transitions (see Table 1),

Table 1: Observational Parameters[a]

Project 2012.1.00681.S		
Continuum (GHz)	279.5	
Beam Size (FWHM)	$0.''46 \times 0.''35$	
P.A. (°)	−83.3	
RMS Noise (mJy beam^{-1})	0.19	
Flux (mJy)	719±72	
Lines	N_2H^+ $J = 3 - 2$	DCO^+ $J = 4 - 3$
Rest frequency (GHz)	279.512	288.144
Beam Size (FWHM)	$0.''75 \times 0.''60$	$0.''58 \times 0.''37$
P.A. (°)	−75.4	−73.2
Channel spacing (km s^{-1})	0.13	0.063
Integrated Flux (Jy km s^{-1})	0.52±0.05	1.34±0.13
Project 2011.1.00010.SV		
Continuum (GHz)	218.3	
Beam Size (FWHM)	$0.''73 \times 0.''57$	
P.A. (°)	73.2	
RMS Noise (mJy beam^{-1})	0.19	
Flux (mJy)	609±61	
Lines	$C^{18}O$ $J = 2 - 1$	^{13}CO $J = 2 - 1$
Rest frequency (GHz)	219.560	220.399
Beam Size (FWHM)	$0.''89 \times 0.''72$	$0.''87 \times 0.''70$
P.A. (°)	82.8	84.3
Channel spacing (km s^{-1})	0.33	0.33
Integrated Flux (Jy km s^{-1})	6.8±0.7	19±2

[a] All quoted values assume natural weighting.

one contained a H_2CO line[1], and the last SPW sampled only the continuum. The nearby quasar J1733-1304 was used for phase and gain calibration with a mean flux density of 1.048 Jy. The visibility data were reduced and calibrated in CASA 4.2.

The continuum visibilities were extracted by averaging the line-free channels. We carried out self-calibration procedures on the continuum as demonstrated in the HD 163296 Science Verification Band 7 CASA Guides, which are available online[2]. We applied the continuum self-calibration

[1] We defer the analysis of H_2CO to future work because the emission distribution can be complicated with respect to the location of the CO snow line (e.g. Loomis et al. 2015).

[2] https://almascience.nrao.edu/almadata/sciver/HD163296Band7

correction to the N_2H^+ $J = 3 - 2$ and DCO^+ $J = 4 - 3$ line data and subtracted the continuum emission in the visibility domain.

To optimize the signal-to-noise ratio of the N_2H^+ channel maps, we applied a Gaussian taper to the visibilities that corresponds to 0.5″ FWHM in the image domain. The resulting synthesized beam for the N_2H^+ $J = 3 - 2$ data cube is 0.″75 × 0.″60, slightly larger than the beam used to observe DCO^+ $J = 4 - 3$, (0.″58 × 0.″37). The integrated fluxes and the beam information are reported in Table 1. We note that this tapering does not affect the model fit procedure that is used to extract the radial abundance profiles of the two species, since that fitting is done in the visibility domain.

We also make use of the ^{13}CO and $C^{18}O$ $J = 2 - 1$ emission toward HD 163296 in the ALMA science verification (SV) program 2011.0.00010.SV. See the observations and data reduction details in Rosenfeld et al. (2013). The continuum and line intensities are also reported in Table 1 and agree with measurements in Rosenfeld et al. (2013).

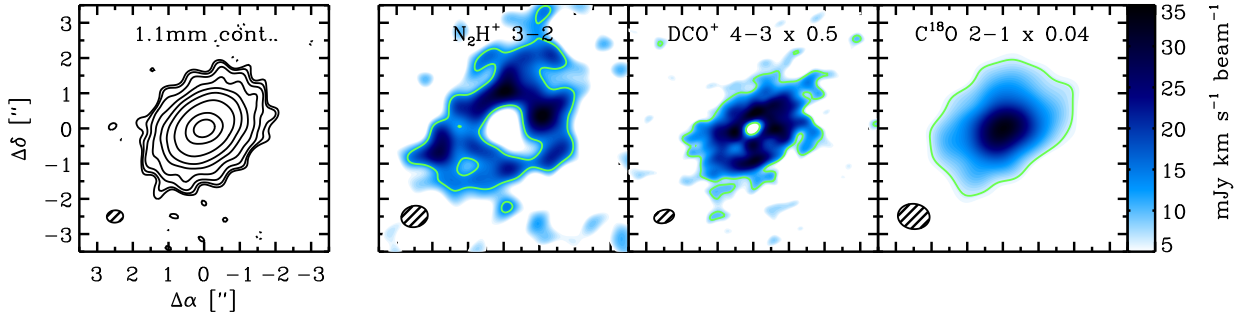

Fig. 1.— Continuum and integrated intensity images of N_2H^+ $J = 3 - 2$, DCO^+ $J = 4 - 3$ and $C^{18}O$ $J = 2 - 1$ toward the disk around HD 163296. The contours in the continuum image are 2σ+[2,4,8,16,...]σ with the continuum $\sigma = 0.19$ mJy beam^{-1}. The green contours in the line images are 3σ except 15σ for $C^{18}O$ $J = 2 - 1$. The integrated line emission scale is shown to the right of the $C^{18}O$ panel. Synthesized beams are drawn in the bottom left corner of each panel.

3. Results

Figure 1 shows the continuum and integrated intensity maps of N_2H^+ $J = 3 - 2$, DCO^+ $J = 4 - 3$ and $C^{18}O$ from the HD 163296 disk. The channel maps used to construct those maps are also shown in the Appendix. The 1.1 mm continuum image in Figure 1 shows centrally peaked emission with an integrated flux density of 719±72 mJy (RMS noise level of 0.19 mJy beam^{-1}), consistent with previous SMA measurements (Qi et al. 2013a). The integrated intensity of N_2H^+ $J = 3 - 2$, 0.52±0.05 Jy km s^{-1}, also agrees well with previous SMA observations (Qi et al. 2013a). The N_2H^+ emission is clearly distributed in a ring (disk inclination at around 44°, see Qi et al. 2011) with an approximate inner edge radius of 0.6 to 0.8″ (based on visual inspection). The DCO^+ emission is

also distributed in a ring, albeit with a substantially smaller inner edge of 0.2 to 0.4″. The DCO^+ emission is also considerably more compact than the N_2H^+ emission. The $C^{18}O$ emission shows centrally peaked emission around the 1.1 mm continuum peak.

In the following sections, we use the spatially and spectrally resolved N_2H^+, DCO^+, and $C^{18}O$ line emission to constrain the abundance profiles of the three molecules, and their relation to one another and the CO snow line.

3.1. N_2H^+ and the CO snow line location

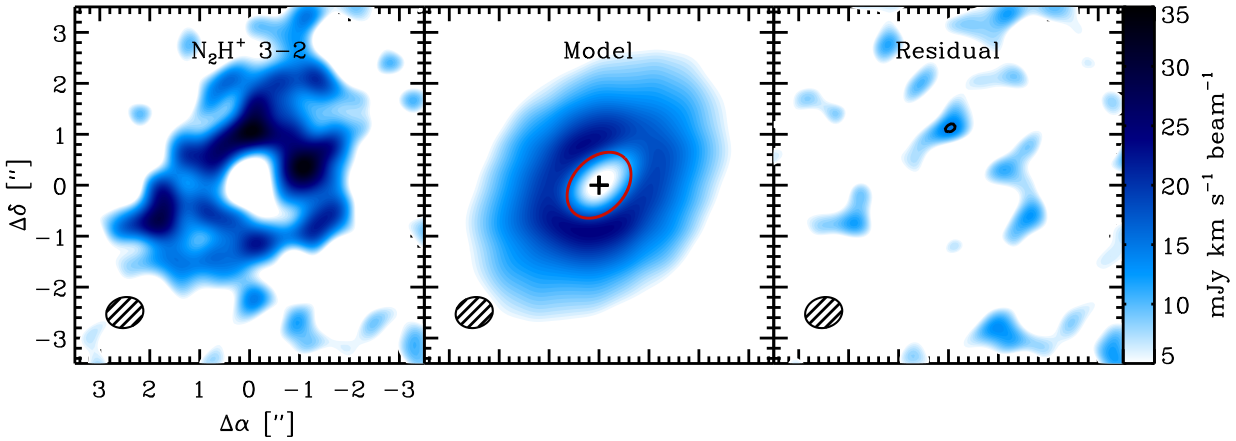

Fig. 2.— N_2H^+ $3-2$ observations, simulated observations of the best-fit N_2H^+ model, and the imaged residuals, calculated from the visibilities. The red ellipse marks the best-fit inner radius of the N_2H^+ ring at 90 AU, the CO snow line in the disk midplane. The residual shows also the contours in steps of 3σ. The integrated line emission scale is shown to the right of the upper right panel. Synthesized beams are drawn in the bottom left corner of each panel.

Based on the simple chemical connection between N_2H^+ abundance and CO depletion, we expect that N_2H^+ emission provides the strongest available constraints on the CO snow line location. We extract the N_2H^+ abundance profile in the HD 163296 disk following the methodology of

Table 2: Fitting results[a]

Transitions	R_{in} (AU)	p	N_{100} (cm^{-2})	R_{out} (AU)	σ_s,σ_m[b]
N_2H^+ $3-2$	90^{+8}_{-6}	$-0.7^{+0.1}_{-0.2}$	$(2.6\pm0.1)\times10^{11}$	500[b]	1,32
DCO^+ $4-3$	40^{+6}_{-3}	$-1.0^{+0.1}_{-0.1}$	$(8.5\pm0.5)\times10^{11}$	290^{+6}_{-8}	1,32

[a]Errors within 3σ.

[b]Fixed parameters.

Qi et al. (2011, 2013b). We adopt the density and temperature disk structure from Qi et al. (2011), which constitutes a physically self-consistent accretion disk model with an exponentially tapered edge that matches the HD 163296 spectral energy distribution and optically thick multi-transition ^{12}CO observations. The N_2H^+ column density profile is parameterized as $N_{100} \times (r/100)^p$ with an inner and outer boundary, where N_{100} is the column density at 100 AU in cm^{-2}, r is the distance from the star in AU, and p is a power-law index. We fit for an inner radius R_{in} and outer radius R_{out} together with the power-law parameters, N_{100} and p.

In the vertical dimension, the N_2H^+ abundance is assumed to be constant between the disk surface (σ_s) and midplane (σ_m) boundaries at each r. These boundaries are described in terms of $\Sigma_{21} = \Sigma_H/(1.59 \times 10^{21}\mathrm{cm}^{-2})$, where Σ_H is the hydrogen column density (measured downward from the disk surface) in the adopted physical model. This simple model approach approximates the outcome of disk chemistry models, which find that most molecules are present in such a layered structure. We fix the vertical boundary values σ_s, σ_m to 1, 32, respectively, as listed in Table 2, based on the chemical models of Aikawa & Nomura (2006, Fig. 8), which shows that the abundances of the common disk molecules HCN and HCO+ are sharply reduced at $\Sigma_{21} < 1$ (the disk surface) and $\Sigma_{21} > 10$ (due to freeze-out in the midplane). Because DCO^+ and N_2H^+ production is enhanced at low temperatures, we expect both molecules to be present deeper toward the midplane than HCN and HCO^+ (e.g. Willacy 2007; Walsh et al. 2010). So we choose a midplane boundary σ_m of 32, the logarithmic mean of 10 and 100. We find that, given the current sensitivity of the data and moderate inclination (44°) of the disk, the fitting results on the radial boundary parameters R_{in} and R_{out} are not sensitive to the choice of these vertical boundaries. Following an initial model optimization, we then also fixed R_{out} to 500 AU (the extent of the CO disk, Qi et al. 2011), since the data provides no constraints on the N_2H^+ beyond a few hundred AU due to a lack of sensitivity.

The best-fit parameter estimates are obtained by minimizing χ^2, the weighted residual of the complex visibilities measured at the (u, v)-spacings sampled by ALMA. We use the two-dimensional Monte Carlo software RATRAN (Hogerheijde & van der Tak 2000) to calculate the radiative transfer and molecular excitation. The collisional rates are adopted from Flower (1999) based on HCO^+ collisional rates with H_2 and the molecular data files are retrieved from the Leiden Atomic and Molecular Database (Schöier et al. 2005).

Figure 2 compares the observed N_2H^+ emission map with the best-fit model (Table 2). See Table 3 of Qi et al. (2011) for other related disk model parameters including disk inclination and orientation. The best-fit model matches the observations very well: the residual image shows no significant emission above the 3σ level. Based on this model, the N_2H^+ column density is 2.6±0.1 $\times 10^{11}$ cm^{-2} at 100 AU and the power-law index is -0.7. The most important parameter in the model fit is R_{in}, since it is associated with the CO snow line location. We find R_{in}=90^{+8}_{-6} AU. Note that this radius is 65 AU interior to the CO snow line location estimated by Qi et al. (2011). The N_2H^+ inner edge corresponds to a midplane temperature of 25 K in the underlying model of the disk structure.

3.2. $C^{18}O$ constraints on the CO snow line

The CO snow line location that would be implied by the N_2H^+ inner ring edge is in clear conflict with the value derived by Qi et al. (2011), which was based on modeling the ^{13}CO line emission. Here we (re-)analyze the spatially resolved CO isotopologue emission from the HD 163296 disk using the same model framework as outlined above and ALMA archival ^{13}CO and $C^{18}O$ data.

As a first step we repeated the analysis presented in Qi et al. (2011) using the new ^{13}CO J=2−1 data from ALMA, with substantially improved sensitivity (Qi et al. (2011) used Submillimeter Array observations). Doing so, we recover the best-fit model presented by Qi et al. (2011), with a CO snow line at 155 AU. Next, we tried to fit the new ALMA $C^{18}O$ J=2−1 data using the same model structure and CO snow line location, but with the fractional abundance of $C^{18}O$ as a free parameter. Figure 3 (top panels) demonstrates that such a model cannot fit the $C^{18}O$ data very well. The model with a 155 AU snow line systematically over-predicts the $C^{18}O$ emission interior to 155 AU and under-predicts it at larger radii, regardless of the level of CO depletion, indicating that there is no sharp drop in the CO abundance at 155 AU. Compared to ^{13}CO, $C^{18}O$ should be less affected by opacity effects and therefore provide a more direct constraint on the CO column density profile.

The failure of the model to reproduce the $C^{18}O$ emission morphology with a fixed 155 AU snow line suggests that ^{13}CO emission is not a robust tracer of CO depletion by freeze-out. One possible explanation of this discrepancy is that the ^{13}CO line is optically thick out to ∼155 AU; the apparent 155 AU snow line inferred by Qi et al. (2011) actually reflects the transition to optically thin emission, with a pronounced intensity drop without a corresponding column density decrease. In order to maintain high ^{13}CO optical depths at such large radii, there must be some midplane gas-phase CO abundance exterior to the CO snow line. Qi et al. (2011) assumed *complete* freeze-out of CO whenever the temperature is below a critical value. However, non-thermal desorption mechanisms (e.g., UV photodesorption) can maintain a relatively large CO fraction in the gas phase (Öberg et al. 2008) at the low densities present in the outer disk.

The $C^{18}O$ isotopologue is expected to be ∼8× less abundant than ^{13}CO, and therefore its emission morphology is much less likely to be affected by these opacity effects. To explore its ability to constrain the CO snow line, we repeated the analysis methodology described by Qi et al. (2011), but now with both the CO freeze-out temperature (T_{CO}) and the CO freeze-out fraction (depletion factor; F_{CO}) as free parameters (while fixing the surface boundary σ_s as 0.79 to keep the problem computationally tractable). The lower boundary (toward midplane) is still governed by T_{CO}, and the abundance of CO drops substantially when $T<T_{CO}$ but not to 0, i.e. no complete freeze-out of CO. We find a best-fit $T_{CO} = 25 - 26$ K, which occurs at a radius of 85–90 AU for the adopted disk structure. The best-fit $C^{18}O$ abundance is 9×10^{-8}, corresponding to CO abundance of 5×10^{-5} assuming an abundance ratio of $CO/C^{18}O$=550, and the depletion factor is about 5. The depletion factor depends on the detailed thermal and non-thermal desorption processes of CO ice across the disk. However, in this model approach, it is fit as a constant and the value of

the depletion factor doesn't affect the derived value of T_{CO} or the location of the CO snow line R_{CO} in our model fit. The bottom panel of Figure 3 shows the $C^{18}O$ column density profile of the best-fit model compared with the original Qi et al. (2011) model. In this model, the optical depth of ^{13}CO $J = 2 - 1$ is about unity at around 155 AU (with ^{13}CO column density around $7{\times}10^{16}$ cm^{-1} assuming $^{13}CO/C^{18}O$ is around 8) , where marks the transition from optically thick to thin for ^{13}CO $J = 2 - 1$ emission. The match of the best-fit model with the $C^{18}O$ data is much improved compared to the original Qi et al. (2011) model (Fig. 3). The fit is not perfect, however; residuals in the inner disk suggest that the simple parametric form used for the CO abundance profile, and/or the adopted disk structure model, are imperfect at the smallest radial scales.

That said, the CO snow line location derived from the $C^{18}O$ emission is in excellent agreement with the N_2H^+ inner ring edge. This again confirms that this chemical signature in the N_2H^+ emission morphology provides a robust tracer of this major volatile snow line. Moreover, the inferred discrepancy between the CO snow line locations derived from the ^{13}CO and $C^{18}O$ emission highlights the potential dangers of using only CO isotopologues to constrain the CO snow line: rapid changes in line opacities can masquerade as snow lines. This latter effect is especially problematic in cold disks where the CO snow line is close to the central star, as well as in very massive disks (as is the case here).

3.3. The DCO^+ abundance profile

We also modeled the DCO^+ $J = 4{-}3$ emission pattern following the same strategy as for N_2H^+. We assumed a different set of vertical boundaries, taking into account model predictions that the DCO^+ abundance should peak at elevated temperatures (above the CO freeze-out temperature) compared to N_2H^+. However, as for N_2H^+, these have little effect on the inner and outer radial boundaries. Figure 4 shows the best-fit model of DCO^+ and how it compares with the data. Similar to N_2H^+, the best-fit model reproduces the data very well. Table 2 summarizes the best-fit parameters. As might be expected given Figure 1, both the inner and outer radial abundance boundaries are smaller for DCO^+ than for N_2H^+, 40 and 290 AU, respectively (compared to 90 and 500 AU for N_2H^+). Contrary to the expectations from models of simple chemical pathways, the outer DCO^+ emission boundary does not coincide with the derived CO snow line location of 90 AU (nor with the previous ^{13}CO-based snow line estimate of 155 AU).

In addition, we explored the sensitivity of the derived DCO^+ radial abundance structure on excitation, employing ALMA Science Verification data for a higher energy transition, $J = 5{-}4$ (see Mathews et al. 2013). With the uncertainties, the derived best-fit model is consistent with what we find here for the J=4−3 transition (the inner boundary is 30 ± 10 AU and the outer boundary is 280 ± 30 AU). Put simply, there is no obvious relationship between the observed radial distribution of DCO^+ emission and the location of the CO snow line.

4. Discussion

4.1. Chemical tracers of CO snow line

N_2H^+, CO isotopologues, and DCO^+ have all been used to chemically image the location of the CO snow line in disks (Qi et al. 2011, 2013b; Mathews et al. 2013). Our analysis of the distributions of N_2H^+, ^{13}CO, $C^{18}O$, and DCO^+ in the disk around HD 163296 shows that the estimates of the CO snow line location from N_2H^+ and the optically thin isotopologue $C^{18}O$ agree: both suggest that CO freeze-out starts at ∼90 AU (in the midplane). By contrast, the utility of ^{13}CO in this effort is limited by opacity effects. The DCO^+ emission does appear as a ring, and its overall emission structure must be related to CO freeze-out since one of its reactants is gas-phase CO. However, neither the inner nor the outer DCO^+ emission edges coincide with the CO snow line location, suggesting a more complicated relationship between CO freeze-out and DCO^+ emission than was proposed by Mathews et al. (2013), perhaps relating to the "higher temperature" chemical channel discussed by Favre et al. (2015).

These data indicate that both N_2H^+ and optically thin CO isotopologues can be used to trace the CO snow line at a disk midplane. Of the two tracers, N_2H^+ provides, perhaps surprisingly, a more robust measure of the snow line location since its defining structure, the location of the inner edge of the N_2H^+ ring, is relatively independent of model assumptions and line opacities.

4.2. CO freeze-out temperature and CO snow line

The CO snow line location depends on both the disk temperature profile and the CO freeze-out temperature. The latter is set by a combination of ice physics and chemistry. The binding energy of CO in pure CO ice is small, resulting in a CO freeze-out/desorption temperature of ∼20 K. CO binds considerably stronger to H_2O ice, which can raise the CO desorption temperature by up to 10 K (Collings et al. 2004). Whether CO will mainly bind to other CO molecules or to H_2O molecules in the icy grain mantle depends on the chemical history of the ice, i.e. whether H_2O and CO co-formed or formed/condensed sequentially (e.g. Garrod & Pauly 2011).

For the HD 163296 disk, we find a CO snow line location that corresponds to a CO freeze-out temperature of 25 K. This is 8 K higher compared to the $T_{\rm CO}$ =17 K found in the disk around TW Hya (Qi et al. 2013b). This difference may be explained by the different chemical histories or evolutionary stages of the two disks. TW Hya is considerably older than HD 163296, and its disk may therefore have experienced more chemical processing that result in more segregated ices, where CO binds mainly to other CO molecules. Higher CO freeze-out temperatures of about 30 K found in embedded protostars (Jørgensen et al. 2015) also support the possible scenario of different ice compositions at different evolutionary stages. The difference in $T_{\rm CO}$ might also be due to different levels of UV ice processing. HD 163296 is a Herbig Ae star, which produces a considerably more luminous UV radiation field compared to TW Hya. This may have resulted in the substantial

production of complex organic molecules in the ices (Öberg et al. 2011b); much like for H_2O, this is expected to increase the CO ice binding energies. A third potential cause is an overall difference in the CO to H_2O abundance in the two disks (i.e., a lower ratio in the HD 163296 disk).

Understanding the origins of the observed difference in CO binding energy is important to interpret Solar System observations, and to predict the locations of CO snow lines in other disks. In the case of a solar type host, a CO freeze-out temperature difference of 8 K is equivalent to a difference of ∼10-20 AU in the CO snow line location (i.e., the difference between Uranus and most comets forming with or without CO). Resolving this question, and constraining how common a high $T_{\rm CO}$ is in disks around solar-type hosts, is therefore key to determining the origin of high O and C abundances in ice giants in the Solar System and to more generally assessing the likelihood of planet formation around the CO snow line. This strongly motivates the need for observational constraints on the distribution of CO snow lines in larger samples of disks.

5. Conclusions

We have presented and analyzed new ALMA Cycle 1 observations of N_2H^+ and DCO^+ emission, along with archival CO isotopologue data toward the disk around HD 163296 with the aim to constrain the CO snow line location. Our key results are:

1. Both the N_2H^+ $J = 3 - 2$ and DCO^+ $J = 4 - 3$ emission exhibit ring-shaped morphologies. The best-fit models for the column density distribution of N_2H^+ has an inner cut-off at 90^{+8}_{-6} AU, which we associate with the CO snow line location. The analogous best-fit model for DCO^+ has an inner abundance boundary at 40^{+6}_{-3} AU and an outer boundary at 290^{+6}_{-8} AU.

2. Analysis of the $C^{18}O$ $J = 2 - 1$ data indicates a CO snow line location that is consistent with the N_2H^+ results, but not with the 155 AU snow line previously derived from ^{13}CO data (Qi et al. 2011). The agreement on snow line location when modeling N_2H^+ and optically thin CO isotopologue emission shows that N_2H^+ is a robust CO snow line tracer, while the relationship between DCO^+ and CO freeze-out in the disk midplane is more complicated.

3. The CO freeze-out temperature in the HD 163296 disk is ∼25 K, which is considerably higher than the 17 K found for the disk around TW Hya. This difference can be explained by different ice compositions and/or morphologies in the two disks. The difference also highlights the need for a survey of CO snow line radii, since their locations will be difficult to predict from theory without more observations.

Facilities: ALMA

This paper makes use of the following ALMA data: ADS/JAO.ALMA#2012.1.00681.S and ADS/JAO.ALMA#201
ALMA is a partnership of ESO (representing its member states), NSF (USA) and NINS (Japan),

together with NRC (Canada) and NSC and ASIAA (Taiwan), in cooperation with the Republic of Chile. The Joint ALMA Observatory is operated by ESO, AUI/NRAO and NAOJ. We acknowledge NASA Origins of Solar Systems grant No. NNX11AK63. This paper is dedicated to the memory of Paola D'Alessio, who was one of the co-Is of project 2012.1.00681.S and passed away in November of 2013.

REFERENCES

Aikawa, Y. & Nomura, H. 2006, ApJ, 642, 1152

Ali-Dib, M., Mousis, O., Petit, J.-M., & Lunine, J. I. 2014, ApJ, 793, 9

Baillié, K., Charnoz, S., & Pantin, E. 2015, A&A, 577, A65

Bergin, E. A., Alves, J., Huard, T., & Lada, C. J. 2002, ApJ, 570, L101

Bergin, E. A., Ciardi, D. R., Lada, C. J., Alves, J., & Lada, E. A. 2001, ApJ, 557, 209

Caselli, P., Walmsley, C. M., Tafalla, M., Dore, L., & Myers, P. C. 1999, ApJ, 523, L165

Chiang, E. & Youdin, A. N. 2010, Annual Review of Earth and Planetary Sciences, 38, 493

Ciesla, F. J. & Cuzzi, J. N. 2006, Icarus, 181, 178

Collings, M. P., Anderson, M. A., Chen, R., et al. 2004, MNRAS, 354, 1133

Favre, C., Bergin, E. A., Cleeves, L. I., et al. 2015, ApJ, 802, L23

Flower, D. R. 1999, MNRAS, 305, 651

Garrod, R. T. & Pauly, T. 2011, ApJ, 735, 15

Gundlach, B., Kilias, S., Beitz, E., & Blum, J. 2011, Icarus, 214, 717

Hogerheijde, M. R. & van der Tak, F. F. S. 2000, A&A, 362, 697

Johansen, A., Oishi, J. S., Low, M.-M. M., et al. 2007, Nature, 448, 1022

Jørgensen, J. K. 2004, A&A, 424, 589

Jørgensen, J. K., Visser, R., Williams, J. P., & Bergin, E. A. 2015, A&A, 579, A23

Loomis, R. A., Cleeves, L. I., Öberg, K. I., Guzman, V. V., & Andrews, S. M. 2015, ApJ, 809, L25

Mathews, G. S., Klaassen, P. D., Juhász, A., et al. 2013, A&A, 557, A132

Mumma, M. J. & Charnley, S. B. 2011, ARA&A, 49, 471

Öberg, K. I., Boogert, A. C. A., Pontoppidan, K. M., et al. 2011a, ApJ, 740, 109

Öberg, K. I., Qi, C., Wilner, D. J., & Andrews, S. M. 2011b, ApJ, 743, 152

Öberg, K. I., van der Marel, N., Kristensen, L. E., & van Dishoeck, E. F. 2011c, ApJ, 740, 14

Öberg, K. I., van Dishoeck, E. F., & Linnartz, H. 2008, in IAU Symposium, Vol. 251, IAU Symposium, ed. S. Kwok & S. Sanford, 449–450

Oka, A., Inoue, A. K., Nakamoto, T., & Honda, M. 2012, ApJ, 747, 138

Qi, C., D'Alessio, P., Öberg, K. I., et al. 2011, ApJ, 740, 84

Qi, C., Öberg, K. I., & Wilner, D. J. 2013a, ApJ, 765, 34

Qi, C., Öberg, K. I., Wilner, D. J., et al. 2013b, Science, 341, 630

Ros, K. & Johansen, A. 2013, A&A, 552, A137

Rosenfeld, K. A., Andrews, S. M., Hughes, A. M., Wilner, D. J., & Qi, C. 2013, ApJ, 774, 16

Schöier, F. L., van der Tak, F. F. S., van Dishoeck, E. F., & Black, J. H. 2005, A&A, 432, 369

Walsh, C., Millar, T. J., & Nomura, H. 2010, ApJ, 722, 1607

Willacy, K. 2007, ApJ, 660, 441

A. Channel images

Figure 5 and 6 show channel maps for N_2H^+ $J = 3 - 2$ and DCO^+ $J = 4 - 3$ and their best-fit models along with the residuals. The best-fit models are described in Table 2.

This preprint was prepared with the AAS LaTeX macros v5.2.

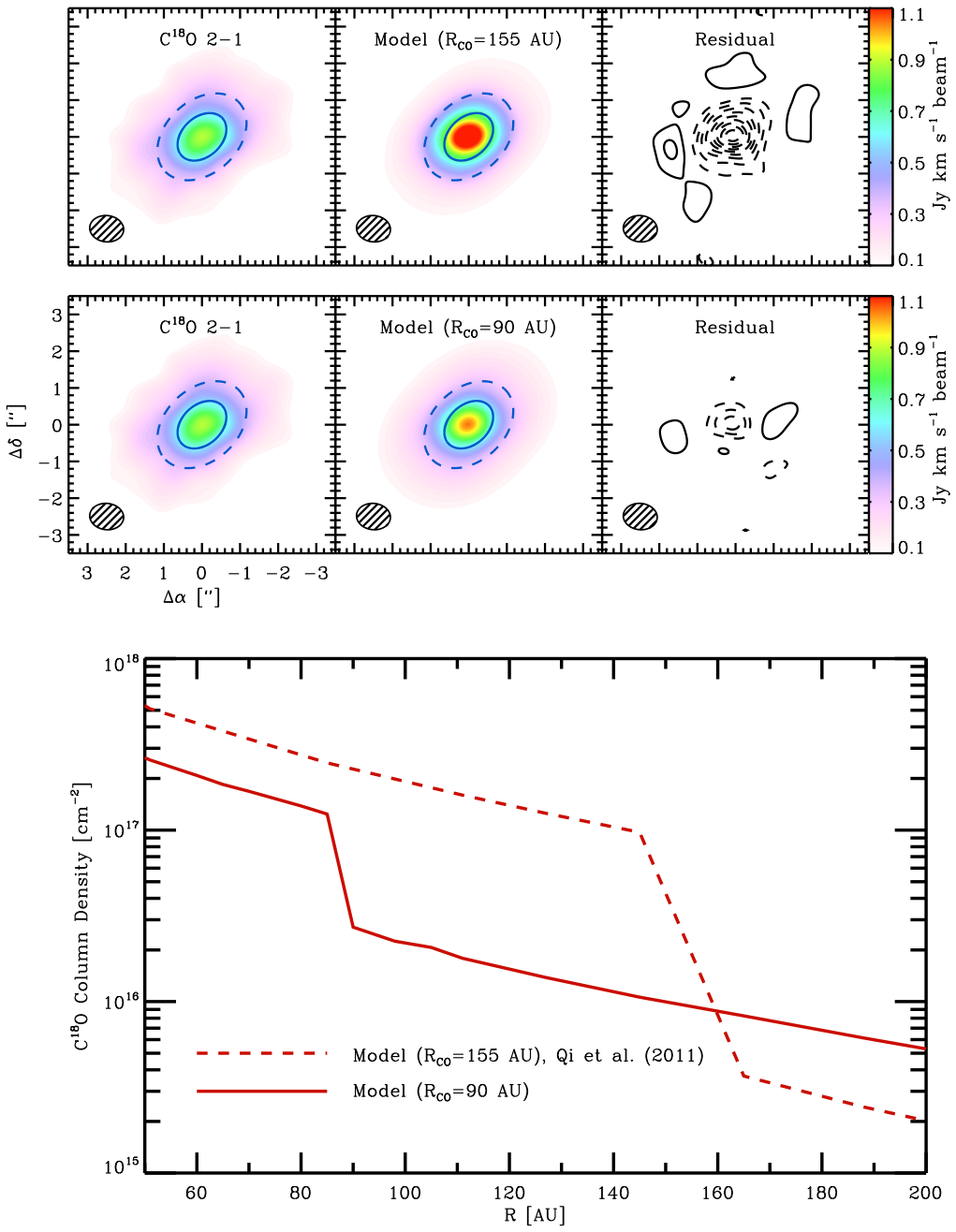

Fig. 3.— Model results for the $C^{18}O$ abundance structure toward HD 163296. *Top panels:* Observations of $C^{18}O$ 2–1 toward HD 162396 (left) together with the modified model based on Qi et al. (2011) with T_{CO}=19 K and R_{CO}=155 AU (upper middle panel) and the best-fit model with T_{CO}=25 K, R_{CO}=90 AU (lower middle panel). The residuals show the contours in steps of 3σ. Solid and dashed blue ellipses mark the radii of 90 AU and 155 AU, respectively. The integrated line emission scale is shown to the right of the panels Synthesized beams are drawn in the bottom left corner of each panel. *Bottom panel:* $C^{18}O$ column density profiles for the two models.

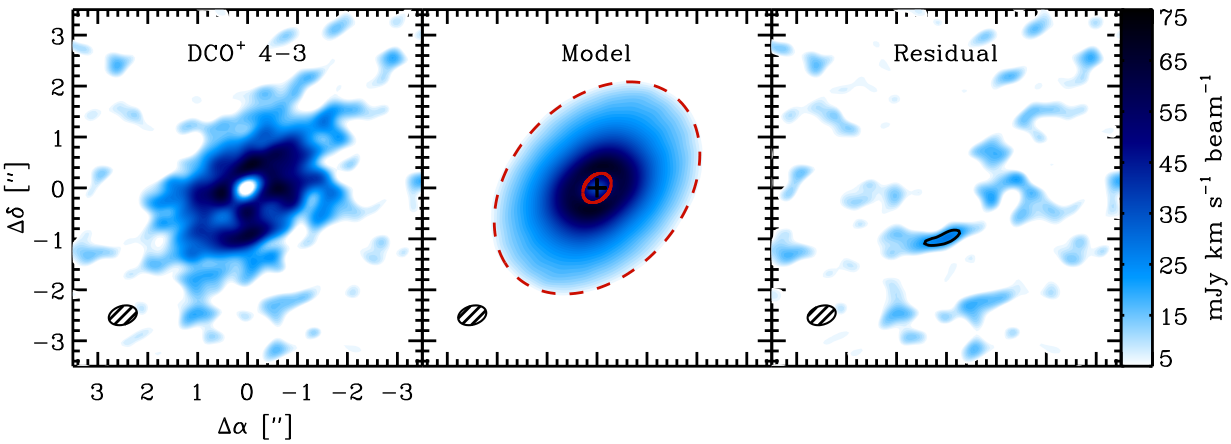

Fig. 4.— Integrated intensity image of DCO^+ $4-3$, simulated image of the best-fit model, and the residual. The red solid and dashed ellipses mark the best-fit inner radius of 40 AU and outer radius of 290 AU of the DCO^+ ring. The residual shows also the contours in steps of 3σ. The integrated line emission scale is shown to the right of the upper right panel. Synthesized beams are drawn in the bottom left corner of each panel.

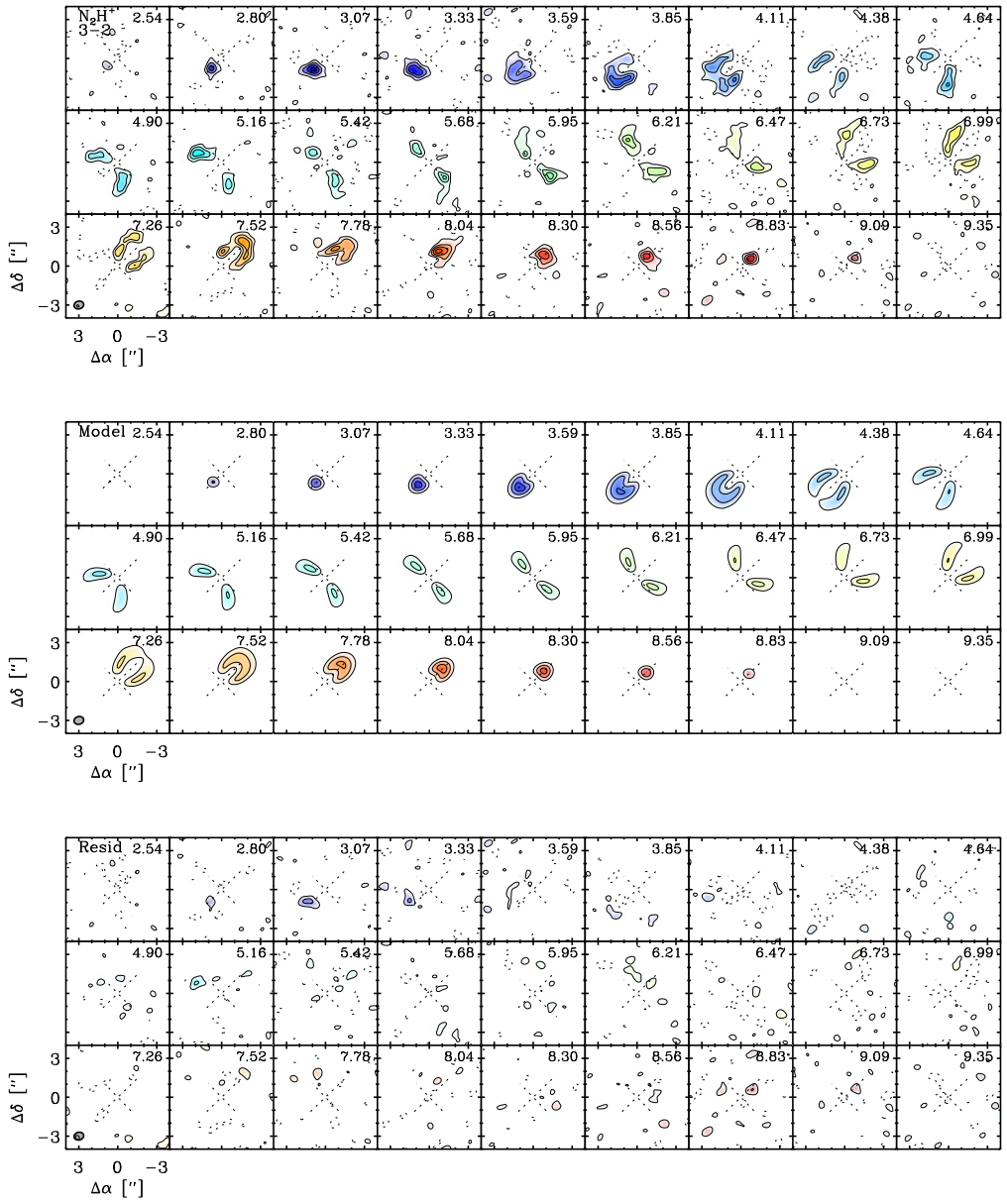

Fig. 5.— Channel maps of the N_2H^+ $J = 3 - 2$ line emission toward the disk of HD 163296. The LSR velocity is indicated in the upper right of each channel, while the synthesized beam size and orientation ($0.''75 \times 0.''60$ at a position angle of $-75.4°$) is indicated in the lower left panel. The contours are 0.0035 (1σ) $\times[2, 4, 6, 8, 10, 12]$ Jy beam^{-1} .

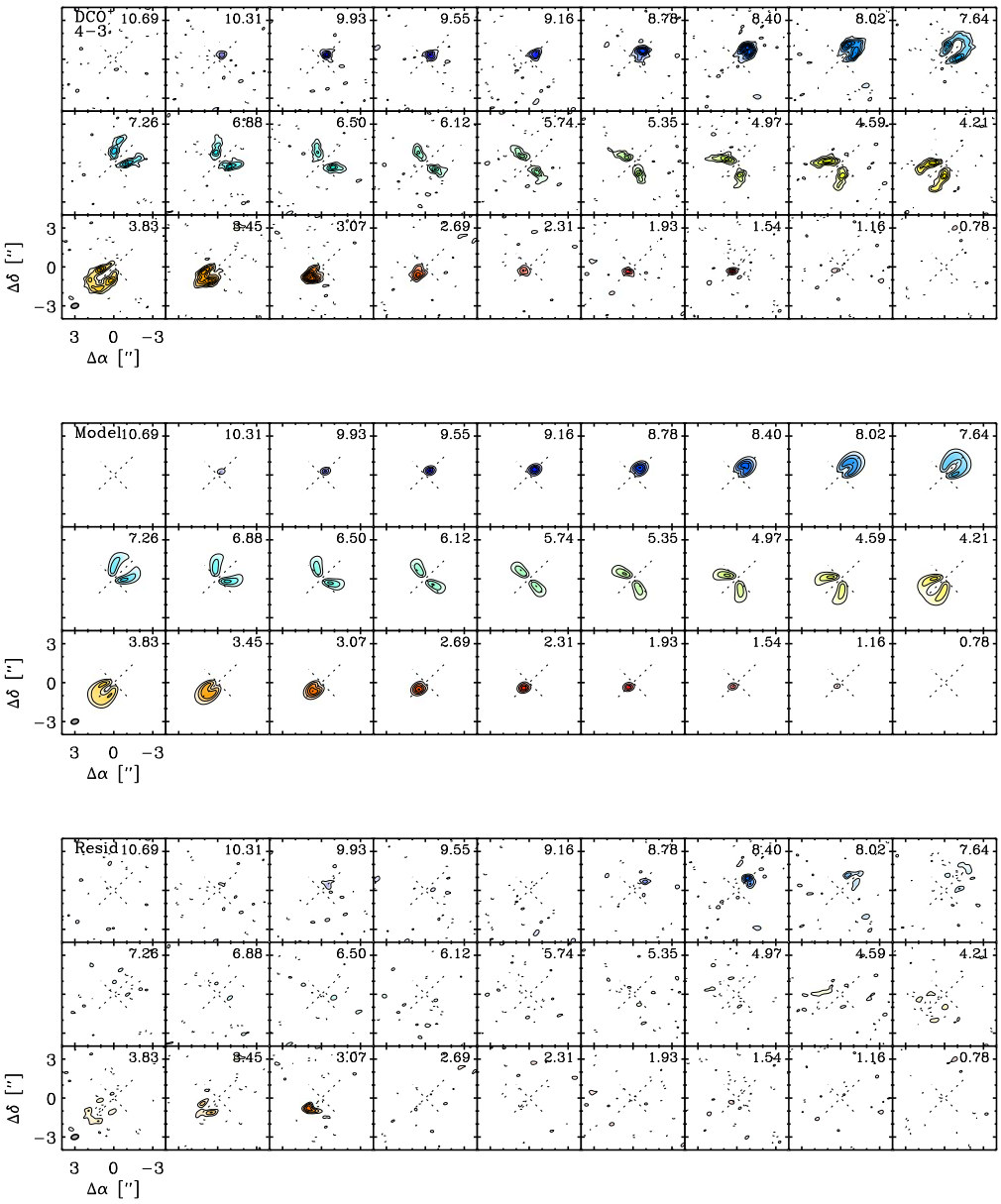

Fig. 6.— Same as Fig 5 but for DCO^+ $J = 4 - 3$ line emission and the synthesized beam size and orientation ($0.''58 \times 0.''37$ at a position angle of $-73.2°$) is indicated in the lower left panel. The contours are 0.04 (1σ) $\times[2, 4, 6, 8, 10, 12, 14, 16]$ Jy beam^{-1} .